

# Low-loss and high index-contrast tantalum pentoxide microring resonators and grating couplers on silicon substrates

Payam Rabiee,<sup>1,2,\*</sup> Ashutosh Rao,<sup>2</sup> Jeff Chiles,<sup>2</sup> Jichi Ma,<sup>2</sup> and Sasan Fathpour<sup>2,3</sup>

<sup>1</sup>Partow Technologies LLC, Orlando, Florida 32816, USA

<sup>2</sup>CREOL, The College of Optics and Photonics, University of Central Florida, Orlando, Florida 32816, USA

<sup>3</sup>Department of Electrical and Computer Engineering, University of Central Florida, Orlando, Florida 32816, USA

\*Corresponding author: pr@partow-tech.com

Received July 11, 2014; accepted August 5, 2014;

posted August 13, 2014 (Doc. ID 216842); published September 11, 2014

A platform for high index-contrast integrated photonics based on tantalum pentoxide submicrometer waveguides on silicon substrates is introduced. The platform allows demonstration of microring resonators with loaded quality factor,  $Q$ , of 67,000 and waveguides with a propagation loss of 4.9 dB/cm. Grating couplers, with an insertion loss of ~6 dB per coupler and 3 dB bandwidth of ~50 nm, are also demonstrated and integrated with microring resonators. © 2014 Optical Society of America

OCIS codes: (130.0130) Integrated optics; (230.4000) Microstructure fabrication; (230.5750) Resonators; (230.7370) Waveguides.

<http://dx.doi.org/10.1364/OL.39.005379>

Tantalum pentoxide ( $\text{Ta}_2\text{O}_5$ ) is an ideal material for integrated photonic devices and circuits. With a high refractive index of ~2.2, microscale waveguides can be achieved on silicon dioxide ( $\text{SiO}_2$ ) bottom cladding layers. The material is transparent from the ultraviolet to the mid-infrared range (~0.15 to ~4  $\mu\text{m}$  wavelength [1]). Doping  $\text{Ta}_2\text{O}_5$  with rare-earth elements has successfully led to integrated lasers [2]. In addition,  $\text{Ta}_2\text{O}_5$  has a refractive index that is matched to lithium niobate (as well as lithium tantalate), which renders fabrication of microscale hybrid photonic devices, such as microring resonators and Mach-Zehnder electro-optic modulators, by combining a  $\text{Ta}_2\text{O}_5$  rib-loading layer with a thin-film lithium niobate slab layer [3].

Furthermore,  $\text{Ta}_2\text{O}_5$  has the potential to become an attractive material for third-order ( $\chi^{(3)}$  effects) nonlinear integrated optics [4,5]. It is noted that silicon has a very high nonlinear index coefficient,  $n_2$ , and has been aggressively pursued. However, silicon nonlinear devices are unfortunately impaired by nonlinear absorptions in the telecommunication wavelengths [6]. Alternative platforms with higher nonlinear figure of merit have been demonstrated on Si substrates [7,8].  $\text{Ta}_2\text{O}_5$  has an  $n_2$  of  $7.23 \times 10^{-19} \text{ m}^2/\text{W}$  [5], which is ~3 and ~6.5 times higher than SiN and Hydex [7], respectively, and is comparable to chalcogenide glasses [8]. Meanwhile, unlike chalcogenide glasses, it does not suffer from low optical damage threshold. Hence, a low-loss submicron  $\text{Ta}_2\text{O}_5$ -on-Si waveguide technology can become a very promising platform for integrated photonics with several applications and directions.

$\text{Ta}_2\text{O}_5$  waveguides have been demonstrated in the past by sputtering the material on a lower-index material, followed by standard lithography and reactive ion etching processes for lateral confinement [2,4]. However, the attainable propagation loss for the sputtered form of the material has been too high and hence prohibitive for practical applications. For instance, a propagation loss of 8.5 dB/cm was reported in very wide (18  $\mu\text{m}$ )

waveguides. In addition, a compact (submicron)  $\text{Ta}_2\text{O}_5$  waveguide platform has been elusive.

Recently, we have demonstrated the first high-index contrast  $\text{Ta}_2\text{O}_5$  submicron waveguides and microring resonators on silicon (Si) substrates, based on the novel approach of selective oxidation of the refractory metal (SORM), Tantalum (Ta) [9]. The attained microring resonators had cross-sectional dimensions as small as ~600 nm  $\times$  ~500 nm, and yet they possessed propagation losses comparable to the mentioned earlier reports on bulky waveguides.

However, the previous fabrication method requires several processing steps and the propagation loss of the compact waveguides is still relatively high (9 dB/cm). Here, a related but more novel fabrication approach is introduced to overcome these and other challenges. The fabrication still relies on oxidation of the refractory metal, Ta, rather than previously pursued direct sputtering of  $\text{Ta}_2\text{O}_5$ . However, critical process modifications and enhancements are incorporated into our SORM approach to improve the performance of various photonic devices.

Specifically, record-low propagation loss (4.9 dB/cm) in submicron waveguides and much closer to rectangular-shaped waveguide cross-section profiles has been achieved. In addition, grating couplers have been demonstrated on  $\text{Ta}_2\text{O}_5$ , for the first time, to more conveniently couple light in and out of the photonic chips. These proof-of-concept demonstrations confirm that a novel versatile low-loss submicron waveguide technology based on  $\text{Ta}_2\text{O}_5$ -on-Si has been established, and it can be employed for a host of passive and active integrated photonic applications.

The modified and enhanced fabrication process proposed here is shown in Fig. 1. It starts with the formation of a slab layer, which can be made by oxidation of a Ta layer. Alternatively, the slab can be a lithium niobate [8], or lithium tantalate, layer formed on a  $\text{SiO}_2$  lower cladding layer on a silicon substrate. Next, a layer of Ta is

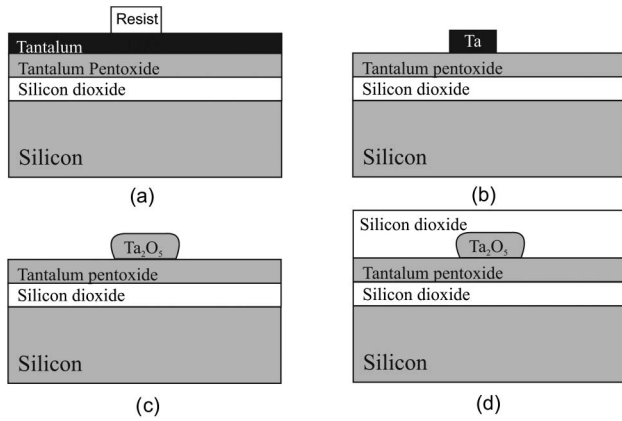


Fig. 1. Processing steps of the proposed waveguide fabrication technique.

deposited on the sample. Photoresist is then spin-coated and patterned using electron-beam lithography. The pattern is transferred to Ta by a chlorine-based selective etching recipe. Since etching Ta can be done highly selectively with respect to the photoresist, it is possible to achieve low sidewall roughness. Next, the unetched Ta region is oxidized in an oven with oxygen flow at  $520^{\circ}\text{C}$  to create a  $\text{Ta}_2\text{O}_5$  layer. Finally, the device can be encapsulated with an optional top cladding layer. If no slab layer is created and the process is started with  $\text{SiO}_2$  on Si wafers, channel  $\text{Ta}_2\text{O}_5$  waveguides can be achieved.

In comparison, our previously demonstrated SORM fabrication process required formation of a trench in a diffusion barrier layer for oxygen, by using  $\text{SiO}_2$  deposited on top of a Ta layer, to selectively oxidize the refractory metal and achieve waveguides [9]. The present fabrication process is simpler, since it does not require the extra steps of deposition of the oxygen diffusion barrier layer and etching.

Figure 2 shows a scanning electron microscopy (SEM) image of a fabricated waveguide cross section based on the present method. During the oxidation process, oxygen diffuses into the Ta layer and the volume of the resulting  $\text{Ta}_2\text{O}_5$  is approximately twice that of the original Ta film. Accordingly, the shape profile in Fig. 2 is achieved. This cross section profile is much closer to a rectangular shape when compared to our previous method [9]. This improvement facilitates better control of the waveguide mode profile. Furthermore, the high selectivity of Ta etching and the inflammation of the layer during oxidation results in smoothed sidewalls. This is another advantage over the previous method, where the selectively oxidized Ta sidewalls could be degraded during the subsequent etching of the remaining Ta. All of these factors have most likely contributed to reduction of the propagation loss (by over two times), compared to those in Ref. [9], as presented below.

To confirm the validity of the new fabrication process, three types of devices (denoted as A, B, and C and schematically shown in Fig. 3) were designed, fabricated, and characterized. First,  $\text{Ta}_2\text{O}_5$  microring resonators were demonstrated (device A). They consist of a 400 nm thick slab layer, a 400 nm thick ridge with a width of 1300 nm. According to our COMSOL simulations, the waveguide is single-mode. Based on this design, negligible radiation

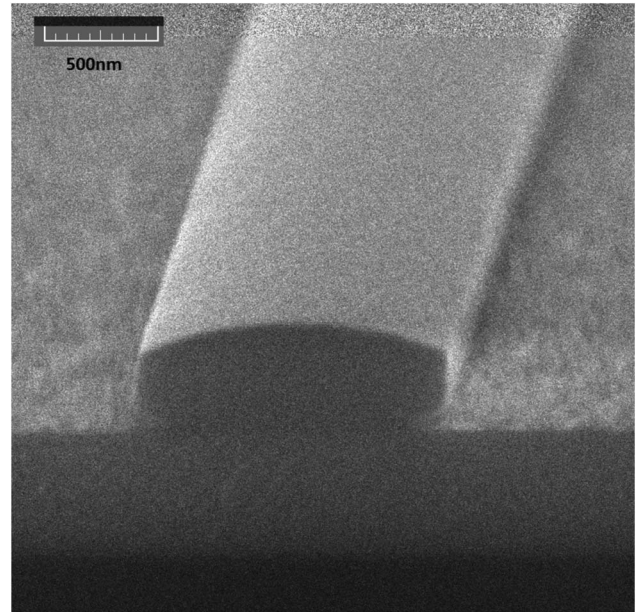


Fig. 2. SEM image of the cross section of the fabricated sub-micrometer waveguide in tantalum pentoxide.

losses can be achieved in microrings with diameters as small as 200  $\mu\text{m}$ . Such devices were fabricated, diced, and polished and the output of a 3 mW tunable semiconductor laser in the 1520–1570 nm range was coupled into them by the end-butt coupling method.

Figure 4 shows the measured output spectrum of an air-clad microresonator with a diameter of 300  $\mu\text{m}$ . Evidently, the microring spectrum is superimposed by strong fringes of the Fabry–Perot cavity formed by the polished facets. Nonetheless, the transmitted spectrum shows a narrow resonance linewidth of 20 pm and a loaded quality factor,  $Q$ , of  $7.75 \times 10^4$ . The measured spectrum was fitted to standard microresonator theoretical model, from which an unloaded  $Q$  of  $1.35 \times 10^5$  and a corresponding propagation loss of 2.9 dB/cm are extracted. The extracted power coupling factor is 2.8%

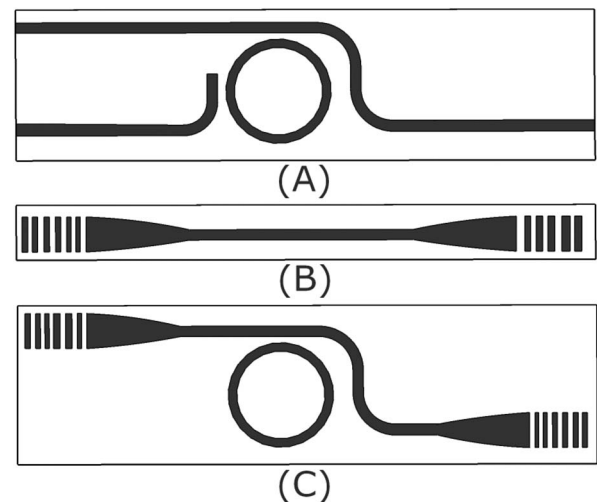


Fig. 3. Top-view schematic of three types of devices reported here: A, end-butt-coupled microring resonators; B, grating couplers; and C, microring resonators integrated with grating couplers.

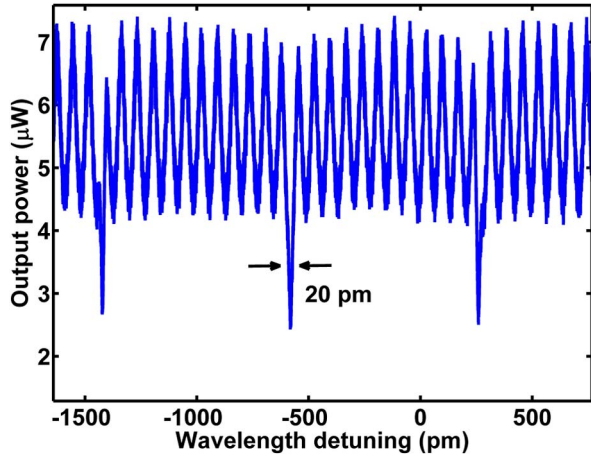


Fig. 4. Output spectrum of Device A, i.e., a microring resonator with a diameter of 300  $\mu\text{m}$  around the measurement wavelength of 1550 nm for an input power of 3 mW.

and hence the device is under-coupled. Because of large Fabry–Perot resonances, this extracted insertion loss is not very accurate and the results presented later for Device C are more reliable. The propagation loss for thin films (slab waveguides) of  $\text{Ta}_2\text{O}_5$ , formed similarly by Ta oxidation and measured using the prism coupling method at  $\sim 1550$  nm, is about 1 dB/cm. Hence, the extra loss measured in the ridge waveguides is most likely attributed to surface scattering effects.

To achieve a versatile integrated photonic platform, efficient couplers are necessary to conveniently couple light in and out of the devices. To address this need, grating couplers (Device B in Fig. 3) were designed and fabricated in the ridge section of an air-clad waveguide with a slab height of 400 nm and a ridge height of 300 nm, which is 100 nm thinner than that of Device A. This thinner ridge height allows achieving stronger coupling efficiency for the coupler.

The grating couplers consist of two sections. The first section incorporates a grating waveguide coupling into a 10.4 by 700 nm  $\text{Ta}_2\text{O}_5$  multimode region from a single-mode optical fiber. The second section is a parabolic-tapered section that couples the multimode region into a much narrower 1300 by 700 nm single-mode region. The grating coupler phase-matches the wave vector of the optical mode propagating in the  $\text{Ta}_2\text{O}_5$  waveguide to that of the free-space Gaussian mode incident at an angle close to perpendicular to the waveguide surface. The periodicity and the filling factor of the grating coupler were varied in order to maximize coupling to the incident Gaussian mode. The period was accordingly varied around 800 nm and the filling factor was varied between 15% and 70%. More details on the design rules and employed model can be found elsewhere [10,11]. The grating couplers were followed by parabolic tapers to convert the 10.4  $\mu\text{m}$  wide mode of the multimode region into the single-mode high-index contrast  $\text{Ta}_2\text{O}_5$  waveguide. The parabolic profile was chosen because of its compactness over linear tapers [12].

Simulations show that such a designed structure couples light into an asymmetric Gaussian mode with a beam diameter of 36 by 10.4  $\mu\text{m}$ . The former value of 36  $\mu\text{m}$  is unfortunately larger than the mode size of

typical single-mode optical fibers ( $\sim 10$   $\mu\text{m}$ ). In comparison, in silicon-on-insulator (SOI) waveguides, because of the larger index of silicon, the coupling becomes stronger and it is easily possible to match to the size of single-mode fibers. This disadvantage of the  $\text{Ta}_2\text{O}_5$  submicron waveguide technology ought to be addressed in future works by a more optimized design of the grating couplers or by inserting another mode-converting element between the gratings and the fibers. Nevertheless, the simulation results suggest that it is possible to achieve a coupling loss as low as 5 dB per coupler with the presented design. This loss value has two comparable components. They are the discussed mode mismatch between optical fibers and the grating coupler, and the inevitable diffraction of the guided field toward the substrate by the grating. The results show that the latter component can be as low as 2 dB per coupler; hence if perfect mode-matching between the coupler and the fiber is achieved, insertion loss as low as 2 dB is possible with this geometry.

The grating couplers were tested by placing two standard single-mode fibers close to perpendicular with respect to the input and output gratings surfaces. Figure 5 shows the insertion loss versus wavelength, with a 12 dB peak insertion loss. Considering that the propagation loss in the few-millimeter long waveguide between the input and output couplers is negligible, a coupling loss of  $\sim 6$  dB is extracted per coupler, which is fairly close to the calculated value of 5 dB.

The measured bandwidth of the coupler spans from  $\sim 1520$  to above 1565 nm (our measurement setup limit), as can be seen in Fig. 5. The measured trend and bandwidth are in general agreement with the simulated results (also presented in Fig. 5). The estimated 3 dB bandwidth of the device is about 50 nm. The discrepancies in the trend and the bandwidth can be attributed to the fact that in the COMSOL-based simulations, simplified 2-D devices with limited area were studied. In addition, there are some ripples in the measured spectrum which probably arise from Fabry–Perot interferences formed between the two optical fibers and are not accounted for in the simulations.

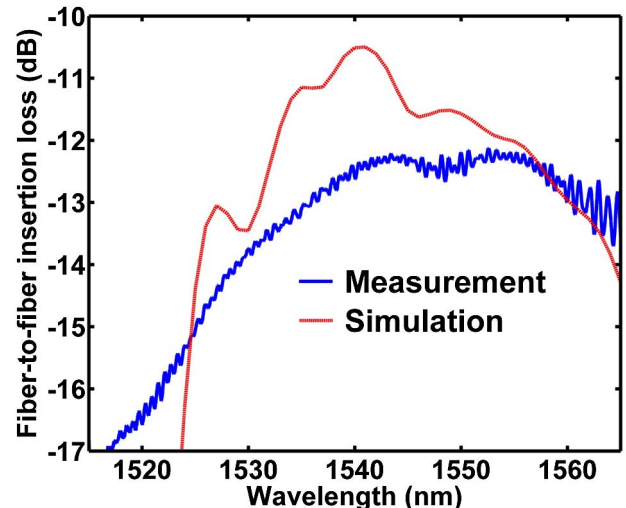


Fig. 5. Measured and simulated transmission spectrum of the grating coupler device.

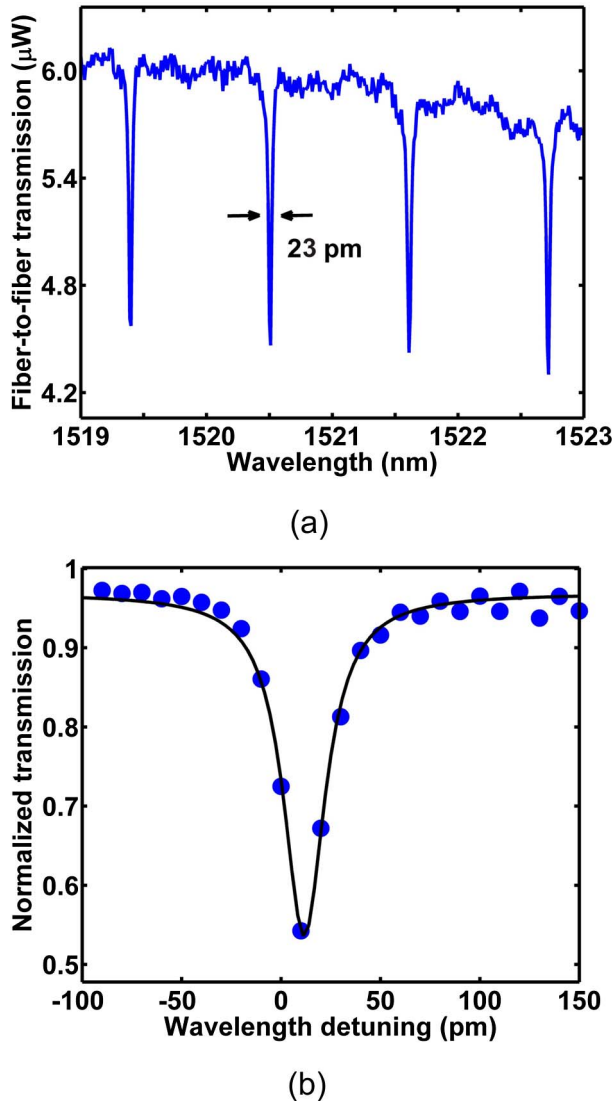


Fig. 6. (a) Output spectrum of the chip for an input power of 3 mW. (b) Zoomed and fitted data to one of the resonances in (a).

Improvement in the attainable transmission spectrum could be possible by more elaborate 3-D designs with the objective of achieving a flatter spectrum over a wider bandwidth and better mode matching with a single-mode fiber. Nevertheless, the present proof-of-concept couplers are efficient enough for practical demonstration of advanced photonic components based on the presented platform.

As a final demonstration, two grating couplers and a microring resonator were integrated in one photonic circuit (denoted as C in Fig. 3). The corresponding waveguide dimensions resemble those of Device A, i.e., 400 nm ridge and 400 nm slab thicknesses and ring diameter of 300 μm. A benzocyclobutene (BCB) top cladding layer is employed in this case to better index-match the medium between the fibers and the gratings and hence eliminate the mentioned Fabry–Perot ripples. The BCB top cladding layer, however, reduces the index contrast between the core and the cladding, and hence the coupled Gaussian mode size becomes even larger than

the previous design with air cladding (Device B). As a result, coupling loss to a single-mode fiber increases to ~11 dB per coupler.

Figure 6(a) shows the output spectrum of Device C. The ring resonator spectrum linewidth is ~23 pm, which is close to the result in Fig. 4 (Device A). Meanwhile, the Fabry–Perot fringes apparent in Figs. 4 and 5 have completely disappeared, as expected in BCB-clad waveguides. The overall measured insertion loss at nonresonant wavelengths is ~24 dB, which is close to the simulated value of 11 dB per coupler.

Figure 6(b) shows a zoomed view of one of the resonances and a fit to the measured data. Based on this plot, a propagation loss of 4.9 dB/cm, corresponding to an unloaded  $Q$  of 80,000 and loaded  $Q$  of 67,000, are extracted. Meanwhile, the extracted power coupling factor of this device is 1.8% and hence it is under-coupled. Since the background Fabry–Perot resonances are absent in this cleaner data, the obtained loss and  $Q$  values are more accurate than those from Fig. 4. The loss values reported here are the lowest in Ta<sub>2</sub>O<sub>5</sub> submicron waveguides to the best of our knowledge.

In conclusion, based on a novel Ta<sub>2</sub>O<sub>5</sub>-on-SiO<sub>2</sub> submicron waveguide fabrication method, record low-loss waveguides (4.9 dB/cm), high- $Q$  (loaded value of 67,000) microring resonators and efficient grating couplers (6 dB loss) are demonstrated for the first time on silicon substrates to the best of our knowledge. Since extremely compact devices can be fabricated using this platform, the waveguide loss is tolerable for practical applications. Grating couplers allow easy characterization of the devices and can potentially be used to couple light in and out of Ta<sub>2</sub>O<sub>5</sub> photonic chips with losses potentially as low as 2 dB.

The work is being supported by the U.S. Office of Naval Research (ONR) Young Investigator Program (YIP) under the Grant No. 11296285.

## References

1. E. Franke, C. L. Trimble, M. J. DeVries, J. A. Woollam, M. Schubert, and F. Frost, *J. Appl. Phys.* **88**, 5166 (2000).
2. B. Unal, C. Y. Tai, D. P. Shepherd, J. S. Wilkinson, N. M. B. Perney, M. C. Netti, and G. J. Parker, *Appl. Phys. Lett.* **86**, 021110 (2005).
3. P. Rabiee, J. Ma, J. Chiles, S. Khan, and S. Fathpour, *Opt. Express* **21**, 25573 (2013).
4. R. Y. Chen, M. D. Charlton, and P. G. Lagoudakis, *Opt. Lett.* **34**, 1135 (2009).
5. C. Y. Tai, J. S. Wilkinson, N. M. B. Perney, M. Caterina Netti, F. Cattaneo, C. E. Finlayson, and J. J. Baumberg, *Opt. Express* **12**, 5110 (2004).
6. B. Jalali and S. Fathpour, *J. Lightwave Technol.* **24**, 4600 (2006).
7. D. J. Moss, R. Morandotti, A. L. Gaeta, and M. Lipson, *Nat. Photonics* **7**, 597 (2013).
8. B. J. Eggleton, B. Luther-Davies, and K. Richardson, *Nat. Photonics* **5**, 141 (2011).
9. P. Rabiee, J. Ma, J. Chiles, S. Khan, and S. Fathpour, *Opt. Express* **21**, 6967 (2013).
10. K. A. Bates, L. Li, R. L. Roncone, and J. Burke, *Appl. Opt.* **32**, 2112 (1993).
11. D. Taillaert, P. Bienstman, and R. Baets, *Opt. Lett.* **29**, 2749 (2004).
12. W. K. Burns, A. F. Milton, and A. B. Lee, *Appl. Phys. Lett.* **30**, 28 (1977).